HARVESTING LARGE ASTRONOMICAL DATA ARCHIVES FOR SPACE DEBRIS OBSERVATIONS

Stephan Hellmich, Elisabeth Rachith, Belén Yu Irureta-Goyena Chang, and Jean-Paul Kneib

Laboratory of astrophysics, École Polytechnique Fédérale de Lausanne (EPFL), Switzerland
Email: stephanhellmich@epfl.ch

ABSTRACT

To obtain a better picture of the evolution and current state of the orbital debris population, we are developing novel methods to efficiently extract observations of satellites, debris and Solar System objects from large astronomical data archives. We are currently evaluating different techniques for detecting the characteristic streaks that these objects cause on the images, such as traditional Hough-transform-based methods and machine-learning approaches. The data we are extracting from these archives contains valuable information that help to better understand the size-frequency distribution of debris particles, which is crucial for the development of strategies to maintain the usability of Earth's orbit for future satellite missions.

We focus not only on detecting orbital debris but also on performing photometric analysis that will allow us to determine the attitude, size and possibly the compositional properties of the observed objects. These properties are of great importance for the selection of targets for active space debris removal missions. In this article, we are presenting the current status of our work and first light curves measured from streaks detected on VST/OmegaCAM observations. Although we focus on space debris, the methods developed are also applied to the detection of near-Earth objects, which leave similar features on the images.

Keywords: Data processing concepts; Light curve photometry.

1. INTRODUCTION

Despite enormous observational effort by numerous space surveillance networks, the population of small (<10 cm) debris particles above low Earth orbit (LEO) is still not well understood. These particles endanger the growing number of satellites in orbit around the Earth. The situation is so dramatic that a collisional cascade, called the Kessler syndrome [1], that would render space around earth unusable for centuries can only be prevented by collision avoidance maneuvers by the operational satellites and by performing active space debris removal (ADR) [2]. These tasks require very precise knowledge about the orbital distribution, size, attitude and physical properties of the resident space objects around Earth, and currently, this knowledge is obtained from observations by the surveillance and tracking networks. Depending on the observation technique, the tracking and surveillance systems cover different size and altitude regimes. The radars currently used for tracking resident space objects can detect particles down to a few millimeters but are limited to about 2000 km altitude (LEO regime). The USAF Space Surveillance Network employs a few meter class optical telescopes that are capable of observing objects beyond LEO but due to the limited number of telescopes, these objects cannot be tracked as reliably as objects in LEO. This results in the debris population of particles up to about 10 cm just above LEO to objects smaller than about 1 m in geostationary orbit (GEO) remaining almost completely unobserved by the surveillance networks[1]. Recently, a survey in the geostationary region was performed with the 2.54 m Isaac Newton Telescope on La Palma, Canary Islands [3]. In eight nights of observations, several hundred particles were identified and it turned out that almost all detections with an estimated size of less than 1 m could not be correlated with any of the cataloged objects. The large number of facilities that are needed to observe small orbital debris on high altitudes make it currently impossible to track these objects as reliably as is the case for debris in LEO. Furthermore, there is only little knowledge on the rotational states and physical characteristics of space debris, properties that are very important for planning active space debris removal missions. While sizes and shapes are known for rocket bodies or other mission related objects, there is a huge amount of fragmentation debris and unidentified objects with unknown physical properties. The rotational state and size of orbital debris can be characterized by photometric observations [4]. However, due to the large amount of observational data needed for photometric analysis, only a few objects have known rotation periods.

The fact that a large fraction the resident space objects are not tracked by the surveillance networks does not mean that they are not observed: there are sev-

[1] https://orbitaldebris.jsc.nasa.gov/measurements/

Table 1. Number of known objects observed with OmegaCAM and DECam in September 2015

	VST/ OmegaCAM	Blanco/ DECam
Number of images	4067	5321
Total observation time	131.8 h	129.8 h
Observed objects	645	2200
Streaks	701	3151
Streaks with start or end	117	680
Streaks with start and end	36	765
Streaks crossing the field	548	1706

Table 2. Orbits of known objects observed with OmegaCAM and DECam in September 2015

Orbit Type	Altitude [km]	VST/ OmegaCAM	Blanco/ DECam
LEO	<2000	464	1533
MEO	2,000 - 35,786	159	535
MOL	600 - 39,700	1	6
GEO	35,786	6	44
HEO	>35,786	15	82

eral large-aperture telescopes with highly advanced wide-field imaging devices that gather large amounts of data every night [5] [6] [7], and of course, satellites and orbital debris have left their traces on the acquired data. However, these observations were not designed for observing satellites and space debris objects but rather to answer fundamental scientific questions in the fields of cosmology, galaxy and star formation and evolution and planetary science. Thus, exploiting their data for space debris research requires sophisticated methods for satellite and debris detection as well as specialized data analysis techniques. In this article we will give an estimation of what we expect to find in the data archives of large aperture survey telescopes, elaborating the debris detection methods that we are currently developing, and show first results that demonstrate the high quality of the data and the advantages of high angular resolution wide field imagers.

2. TREASURES TO BE RECOVERED IN LARGE ASTRONOMICAL DATA ARCHIVES

We are currently focusing on the publicly available data archives of two survey telescopes: the 2.65 m ESO VLT Survey Telescope at Cerro Paranal and the 4 m Blanco Telescope at Cerro Tololo. VST is equipped with OmegaCAM, a 300 Megapixel wide-field optical camera, consisting of 32 individual CCDs that covers one square degree with a resolution of 0.2 arcsec per pixel [8]. The main instrument of the Blanco telescope is the Dark Energy Survey Camera (DECam) that consists of 62 individual CCDs, making up an image of 520 Megapixel that covers 3 square degrees at a scale of 0.26 arcsec per pixel [9]. OmegaCAM was commissioned in 2011 and DECam followed in 2012, and the combined data acquired with these instruments over the last decade consist of almost one million individual science exposures. This corresponds to 3.4 years of continuous exposure time and results in over 1 Petabyte of data.

To give an estimation of what we expect to find in these archives, we can combine the catalog that contains the orbits of known satellites and debris with the observing history of the telescopes. Therefore, we randomly selected one month of observations from the OmegaCAM and DECam archives (September 2015) and combined the pointing history with the orbital elements in the space track catalog at the same epoch in order to determine how many known objects crossed the observed fields and were illuminated by the sun at the time of observation. The results of this analysis are shown in Table 1. Due to the larger field of view, there are more objects observed with DECam than with OmegaCAM. Furthermore, because some objects were observed multiple times, the number of streaks is higher than the number of observed objects. Multiple observations of the same object are especially useful for determining the rotation period. Space debris cover a wide range of rotation periods with the fastest objects spinning at a few revolutions per second [10] [11]. In our case, the exposure time places an upper limit on the duration of each observation and thus the maximum rotation period we can detect from a single observation. Streaks with starting and ending points on the image are observed for the entire exposure time (usually between 30 and 300 s) while streaks with a recorded start or end or streaks that cross the whole image are observed for a shorter time, accordingly. This means that for objects with low tumbling rates, only a fraction of the period may be observed during a single exposure, making period determination impossible. However, by combining the light curves from multiple exposures of the same object we will be able to identify tumbling periods longer than the duration of a single observation. As can be seen in Table 2, most of the observed objects were in LEO and thus have high angular velocities, causing the streaks to cross the whole field which means that the exact observation time is unknown. Still, astrometric and photometric measurements of these streaks can still be made by fitting the orbit to match the streak in order to determine the observation time.

This estimation is based only on the known objects. However, because the catalogs are becoming more and more incomplete with increasing altitude and decreasing object size, we expect to find a lot of unknown objects. In order to demonstrate the capabilities of the instruments and to show how the data in the archives would complement the existing catalogs, we determined the detection limits

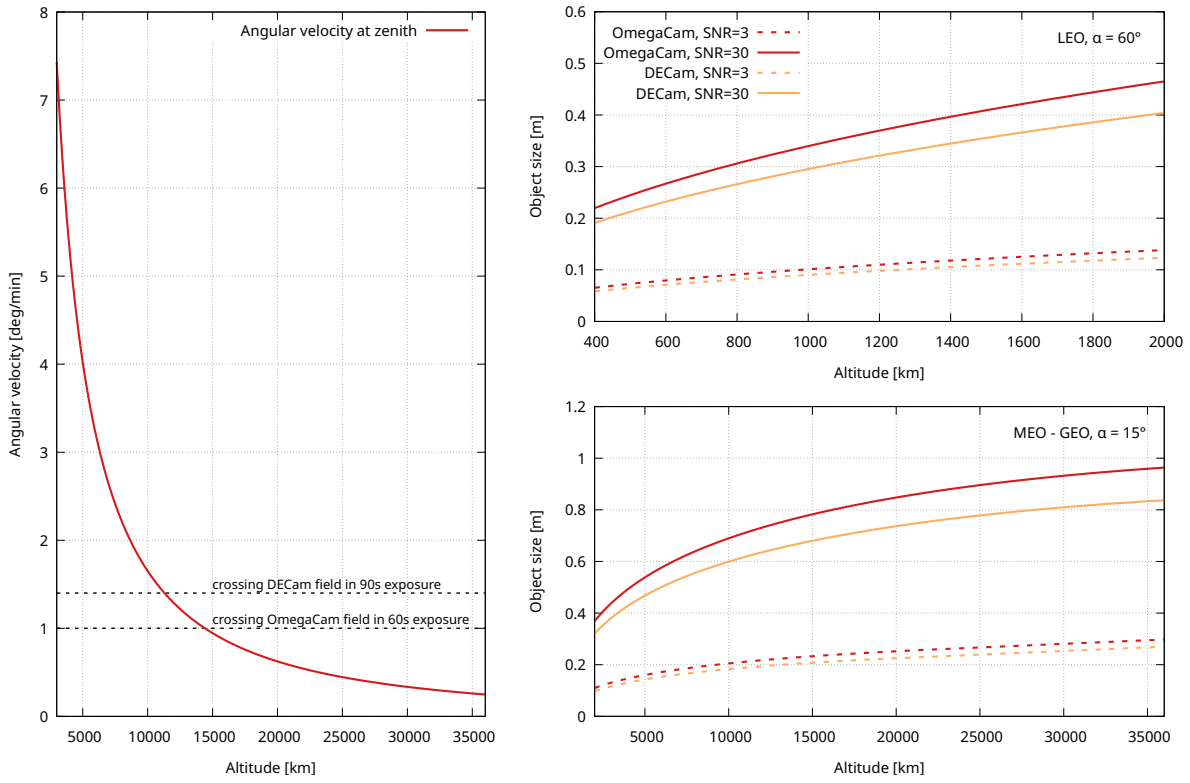

Figure 1. Left: Angular velocity at zenith for a circular orbit over orbital altitude. Right: Size of an object causing a streak with SNR=3 (dashed lines) and SNR=30 (solid lines) over altitude at different orbital regimes

for both telescopes. The brightness of a debris particle on an astronomical image depends on the characteristics of the telescope and the detector, the size and orbit of the observed particle, its distance to the observer and the solar phase angle at the time of observation, the reflectivity of the surface material as well as other observational circumstances like zenith distance, atmospheric conditions, lunar elongation and moon phase. While distance and orbit define the apparent angular velocity, phase angle and reflectivity determine how much sunlight is reflected towards the observer. Depending on the airmass, a part of that light is absorbed by the atmosphere which decreases the signal on the detector. The apparent brightness of a particle is defined as

$$m_{app} = -m_{sun} - 2.5\log(A\rho F(\alpha)) + 5\log(r) + \chi X$$

where m_{sun} is the magnitude of the Sun, A the cross-sectional area of the observed object, ρ the albedo describing the reflectivity, α the phase angle, r the range between object and observer (in the same units as A), χ the athmospheric extincion in mag/airmass and X the airmass. The phase function ($F(\alpha)$) for a diffuse sphere is [12]:

$$F(\alpha) = \frac{2}{3\pi^2}((\pi - \alpha)\cos\alpha + \sin\alpha)$$

and the airmass can be computed from the zenith distance z as

$$X = \frac{1}{\sin(h + 244/(165 + 47h^{1.1}))}$$

where $h = \pi - z$ is the apparent altitude. Blurring due to atmospheric turbulence (seeing) causes the light to be scattered over multiple pixels on the detector, reducing the signal to noise ratio (SNR). Also, as the object is moving across the detector during the exposure, its signal is distributed over a large area, resulting in the SNR to be further decreased. Finally, Lunar elongation and Moon phase determine the background sky brightness [13] and thus also impact the SNR. In order to estimate the SNR of a target on OmegaCAM and DECam, the apparent magnitude m_{app} of the debris particle can be converted to a corresponding flux N_* in e^-/s on the detector using the flux of a mag 20 source (N_{20}) as a reference.

$$N_* = N_{20}10^{-(m_{app}-20)/2.5}$$

The SNR is then defined as:

$$SNR = \frac{N_* t_{tar}}{\sqrt{N_* t_{tar} + S n_{pix} t_{exp} + n_{pix} R^2}}$$

where t_{tar} is the time the target spends in the measurement aperture (defined by its angular velocity), t_{exp} the total exposure time of the image, S the flux due to the background sky brightness, n_{pix} the number of pixels in the seeing dependent measurement aperture and R the readout noise per pixel. Note that this definition of SNR does not correspond to the integrated SNR for the whole streak but is rather intended to indicate how bright the streak will appear above the background of the image. Combining all these factors, an estimation on the size limit for the objects that we can expect to find in the archives can be made. The left panel of figure 1 shows the angular velocity as a function of the orbital altitude, assuming a circular orbit and observation at zenith (where the velocity is at maximum). Objects with angular velocities below the dashed lines do not cross the entire field of a 90 s DECam exposure and a 60 s OmegaCAM exposure, respectively (exposure times that are representing typical values used). For streaks that have start and end point recorded, astrometric and photometric measurements can be made even if the object is unknown, as the exact observation time is determined.

The results for the estimation of the smallest objects that we expect to detect in the OmegaCAM and DECam archives are shown in the right panel of figure 1. An albedo of 0.175 [14] is assumed and the objects are considered to be spherical and to give a lower limit of the objects that can be detected, the target is assumed observed at zenith (1 airmass) in a moonless night with a seeing of 1 acrsecond in the r band. The exposure times where again assumed to be 60 s and 90 s for OmegaCAM and DECam, respectively. Due to geometric constraints, objects in LEO can only be observed at high phase angles while objects at higher altitudes are observable at lower phase angles resulting in more light being reflected towards the observer. To estimate the detection limit, a phase angle of 60 degrees is assumed for the LEO regime while for objects at higher altitudes a lower value of 15 degrees is used. A streak with a brightness corresponding to an SNR=3 should be just bright enough to be detected and streaks above SNR=30 will allow photometric measurements to obtain light curves. Figure 2 demonstrates how bright streaks of different SNR would appear on an image. As can be seen in the right panel of Figure 1, we expect to detect objects down to about 7 to 14 cm in LEO, while in GEO we expect to detect particles as small as 30 cm. These results may seem counter intuitive: As sensitivity drops with the square of range, one might expect the detection limit would increase much steeper. However, due to the fact that the angular velocity decreases with orbital altitude, the flux of the target is distributed over a smaller number of pixels, resulting in a lower t_{tar}/t_{exp} ratio and thus SNR decreases slower.

This estimate clearly shows the great potential that astronomical data archives from large aperture telescopes holds for studying space debris. However, sophisticated image processing techniques are needed to cope with the huge amount of data. Our goal is to develop a processing pipeline that can extract and analyze space debris observations from the archives in a fully automated manner.

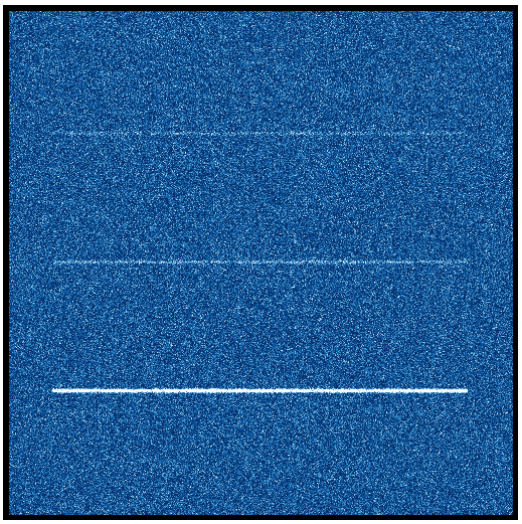

Figure 2. Streaks with SNR of 3, 5 and 30.

Furthermore, the pipeline should be scalable so that it can be applied to the data from next-generation survey telescopes, such as the Large Synoptic Survey Telescope (LSST) [15].

3. DETECTION TECHNIQUES

Several methods exist for the detection of straight lines on images, and more particularly for the detection of space debris tracks on astronomical images. Most of these methods are based on a morphological analysis of the image and the use of a Hough or Radon transform algorithm such as in the work of [16], [17] or [18]. A first analysis of the VST/OmegaCAM images was performed using an algorithm developed by us and based on the Hough transform. The algorithm, as could be expected from previous research, is effective for the detection of space debris tracks in most cases, but suffers from several important limitations.

- The algorithm is poorly performing for the detection of low SNR traces.
- Multiple defects are present in the images, in particular due to diffraction peaks of the brightest stars, bad columns or saturated pixels and the algorithm is not robust in the differentiation of these elements from the true space debris tracks, generating a large number of false positives.
- Despite many efforts to increase the efficiency of this type of algorithm, morphological methods using Hough or Radon transforms are computationally expensive and do not allow for the analysis of the entire OmegaCAM or DECam archive in a reasonable time.

Albeit most detection techniques for satellites and space debris are applicable to asteroid detection, there have

been specific efforts aimed at finding Near Earth Objects (NEOs), which are usually much slower objects (and hence, leave shorter traces on the long-exposure images).

- In this regard, we should remark the work of [19] for detecting asteroids using the Zwicky Transient Facility (ZTF). Their algorithm *DeepStreaks* breaks down the problem of identifying streaks into three simpler problems with three different groups of classifiers: one that finds all streak-like objects, one that finds all short-streak-like objects, and one that finds real streaks. With this approach, they achieved high levels of completeness and relatively low false-positive rates compared to some previous ZTF algorithms [20], but they still rely on human visual inspection to discard the remaining false positives.
- Besides ground observations, there have also been significant developments focused on exploiting data from space telescopes. More specifically, the upcoming mission of the European Space Agency (ESA), *Euclid*, will be orbiting the second Lagrangian point, and will thus be able to observe a range of Solar System objects, mainly main-belt asteroids and transneptunian objects. As a result, ESA has developed a dedicated software, *StreakDet* [21], to identify moving objects in the field of view. However, perhaps its main limitation is the extremely high rate of false positives, which can only be reduced using other methods.
- Other methods for asteroid detection in *Euclid* include the machine-learning algorithm developed by [22], which, despite its high performance, can only confirm the presence of an asteroid in an image, rather than detect it.

With this in mind, we decided to look at other methods for the detection of streaky features in astronomical images. Two algorithms are being developed, one for space debris detection and the other for NEO detection. The two problems, although similar in their linear characteristics, differ in several points. The tracks left by space debris and satellites are long and cross in most cases the whole detector, consequently leaving the beginning and end of the tracks outside the detection area. Moreover, the variations in light intensity, thickness and shape are more pronounced in the case of space debris than in the case of NEOs.

Space debris detection Our current algorithm for the detection of satellites and space debris is based on the HT-LCNN neural network devoloped by Lin et al. [23]. The algorithm is a convolutional neural network with a trainable Hough transform prior. The structure of the neural network is such that the Hough transform block allows the learning of the global features of the image, i.e. the location of the lines to be detected, while the convolutional layers focus on the learning of the local features. The algorithm is initially intended for edge detection in buildings and interior images, and can be used for automatic orientation of smart objects, but has proven to be very promising for the detection of streaks in astronomical images. The main advantages of a machine-learning method over the more traditional morphological tools are the improved versatility for the detection of various shapes and intensities of streaks as well as the rapidity of the algorithms, much less computationally demanding once the neural network has been trained. Promising initial tests have been conducted and a new dataset of 7168 individual images from the VST/OmagCAM is currently under preparation for the training of the algorithm.

NEO detection Our current algorithm for finding NEOs is based on a modified TernausNet architecture [24], which is, in turn, adapted from the well-established U-Net architecture [25]. This type of networks show a strong performance for pixel-wise segmentation, not only allowing for the detection of a streak in a given image, but also returning precise information on its position within the image. Such information is key to subsequently calculate astrometric and photometric parameters that define the asteroid. More specifically, when fed a raw astronomical image, the algorithm conveys in a heatmap the probability of presence of the asteroid streak. Furthermore, to improve the performance of the model during training, the loss is based on a distance criterion from each pixel to the streak. To cover each image as a whole, a window sliding across the full image will be used.

4. LIGHTCURVE PHOTOMETRY

4.1. Image calibration

The OmegaCAM and DECam archives contain various data products that are reflecting the individual requirements of the different surveys done with the instruments. Most of the high level image data products are combined images from dithered exposures to eliminate the gaps between the individual CCDs of the detectors. Because transient objects such as space debris and solar system objects are not present in these higher level data products, we decided to start from the raw data and perform our own calibration. All data required for calibration is stored along with the raw science images in the archives. To calibrate the data processed in this work, we median combined all available bias and flat field exposures that were acquired in the same filter as the observations from the same night as the observation and used these median frames to perform the calibration. A coarse astrometric solution is already stored in the metadata of the images. We use this information to improve the astrometry by matching the images to the GAIA DR2 photometric star catalog.

The large amount of data in the archive places high requirements on the speed of processing pipeline. Each in-

dividual processing step needs to be optimized to achieve acceptable overall processing time. Radiometric calibration is mainly limited by disk throughput capacity. Using cfitsio [2] for data access and performing data manipulation in parallel whenever possible, we achieved computation times of less then 30 s to combine the master calibration frames out of 10 individual bias or flat field exposures and calibration of a single image takes less than 4 s. For star catalog matching, we decided to implement a parallel version of the optimistic pattern matching algorithm described in [26]. This method requires less than a second to match all 32 frames of a single OmegaCAM image (provided that the star catalog is locally stored). These processing times are archived with a consumer laptop equipped with a PCIe 4.0 solid state disk and 4 core CPU. Calibrating the whole OmegaCAM data archive on this computer would take about 21 days.

4.2. Photometric data reduction

One goal of our work is to determine the rotational and physical characteristics of the observed orbital debris. The information needed for this task can be extracted from photometric observations. The amount of light that is reflected from the observed object to the observer depends on the illumination geometry, the rotational phase and the object's shape and surface properties. Acquiring and examining series of brightness measurements, called light curves, makes it possible to draw conclusions about these properties even if the object is not resolved. Light curve analysis is a very power full tool to study unresolved observations and has many applications in astronomy, ranging from characterizing solar system objects [27], searching for exoplanets [28] and variable stars [29]. For our analysis, we are employing the Fourier Analysis of Light Curves (FALC) algorithm [30], that applies a least-squares fit of a Fourier polynomial to the data. This technique is considered the standard method for rotation period determination of asteroids.

To obtain the light curves, we are using a similar approach as in [31]. The intensity profile of a streak is retrieved by placing a series of rectangular apertures along the streak and measuring the flux received from the target in each aperture. We decided to use Photutils[3] to measure the fluxes, a tool that uses similar source extraction and background estimation algorithm than SEXtractor and allows user defined aperture shapes and forced photometry on user defined image coordinates. The time stamp of each measurement is derived from the observation time and the target's apparent angular velocity, computed from its orbital elements. The angular velocity also defines the exposure time of each measurement (the time the target spends in each measurement aperture). Knowing the exposure time allows us to obtain the apparent magnitude of the target on an absolute scale. Therefore, a set of high SNR photometric reference stars on the same field is selected from the GAIA DR2 catalog. Conversion of the magnitudes from the GAIA system to the observed band was done using the relations in [32]. Only stars with a similar color index as the Sun (V-R = 0.5 $\pm$ 0.1) were chosen. Outliers were rejected by combining the selected stars to a master reference star that was then used to compute the expected magnitude for each individual star. Reference stars with a magnitude deviation of more than 3σ from the expected value were rejected. This procedure resulted in 19 to 25 photometric reference stars for each CCD and allowed a robust absolute magnitude determination with an error of a few hundredths of a magnitude. From these reference stars, the magnitudes for each measurement were calculated, accounting for the corresponding exposure time that is defined by the angular velocity of the observed object and the aperture width. Apertures contaminated by background stars or image artifacts were manually excluded.

[2] https://heasarc.gsfc.nasa.gov/fitsio/

[3] https://photutils.readthedocs.io/en/stable/

5. FIRST RESULTS

5.1. 2012-009B (ATLAS 5 CENTAUR R/B)

While annotating the data for training, we noticed a very prominent but not saturated streak that we were able to identify as 2012-009B, a Centaur upper stage of an Atlas 5 Launcher. The object is on an elliptical orbit with a perigee of 3,235 km and an apogee of 35,247 km. It was observed on 2022/05/27 at a distance of 29515 km from VST. The object was in the field at the start of the exposure and crossed eight CCDs of the detector while exposing, resulting in a total duration of the observation of 244 s. We obtained a total of 927 data points from the eight individual light curves.

The search for the fundamental frequency resulted only in a poor fit. Investigating the residuals revealed that there is very likely more than one frequency present in the light curve which usually is an indicator for non principal axis rotation. The implementation of the FLAC algorithm that we are using is capable to search for a second frequency, a feature that can be used to detect and characterize mutual occultation events in binary asteroid systems. This is achieved by employing the FALC algorithm to the residuals of the fit to the most prominent frequency and then subtracting this second fit from the first one [33]. The result of the two period search is shown in Figure 3. The main period (upper plot) is 36.72 s with an amplitude of 2.9 magnitudes. We were not able to detect a clear second frequency with the data reduction method that we used. The lower plot of Figure 3 contains the best fit for the secondary frequency. However, the residuals indicate that there are short- and long-period variations and that the method could not uniquely identify any of the frequencies involved. The solution we found suggests that the period around the shortest axis of rotation is 36.76 s but we will need to employ more sophisticated methods such as the WINDOWCLEAN algorithm [34] to properly interpret the data. Nevertheless the result clearly demonstrate the high quality of the photometry that we can ex-

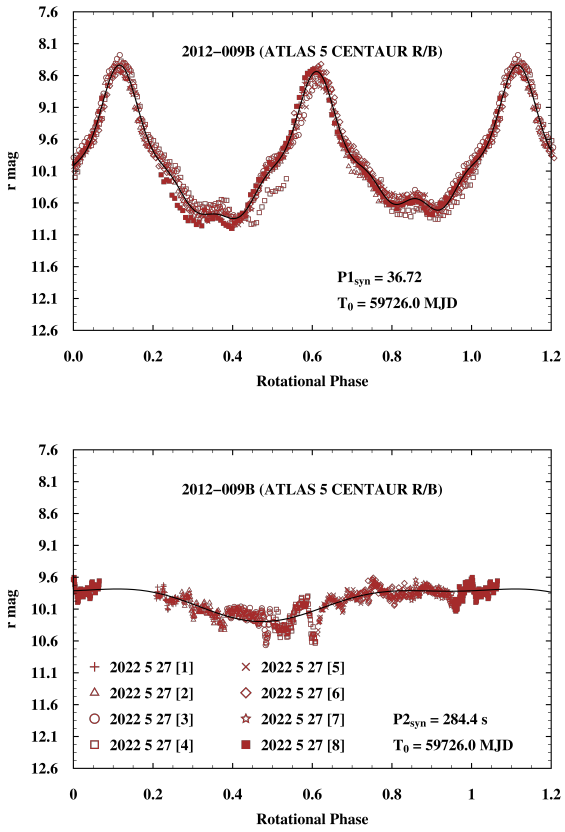

Figure 3. Two period fit of the eight light curves extracted from the streaks of 2012-009B.

pect to find in the OmegaCAM archive.

5.2. 2004-031B (BREEZE-M R/B)

This object, tank of a Proton-M launcher, was observed on 2022/06/09, only a few days after 2012-009B. It also resides on an elliptical orbit with an apogee of 3305 km and a perigee of 35424 km and was at a range of 22688 km while it was observed. The faint streaks that it caused on three CCDs of the detector showed an intensity profile that indicated fast rotation. The duration of the observation was 40 s. Sampling the intensity along the streaks with a rate of 50 ms resulted in as much as 712 data points and allowed us to determine a rotation period of 0.84 s with an amplitude of 1.1 magnitudes. The resulting phase plot is shown in Figure 4. The high sampling rate at a magnitude of 12.76 resulted in a reduced SNR, causing uncertainties in the range of 0.1 to 0.3 magnitudes.

5.3. 2010-006C (BREEZE-M DEB)

On the same image where we found 2004-031B, we identified another object, classified as a debris particle origi-

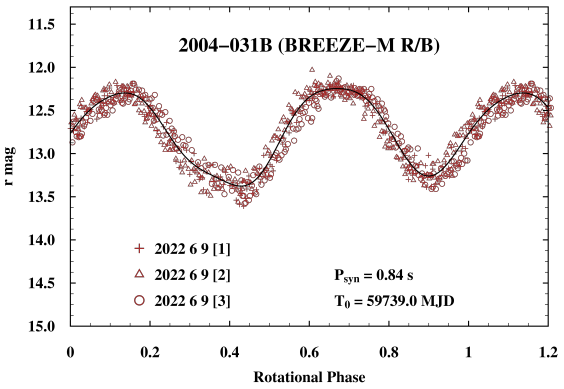

Figure 4. Phase plot of the three streaks caused by 2004-031B.

nating from a Proton-M rocket. With a perigee of 460 km and an apogee of 35784 km it is crossing a large part of the LEO regime. It was observed for 57.5 s at a range of 37280 km and left steaks on two CCDs of OmegaCAM. Sampling the light curve of 2010-006C at a rate of 0.5 s resulted in 74 measurements with uncertainties of about 0.03 magnitudes. Analyzing the data, we were not able to identify the period of the light curve (Figure 5). However, if we identify another observation of this object in the archive, we will search for period using the combined light curves from the individual observations.

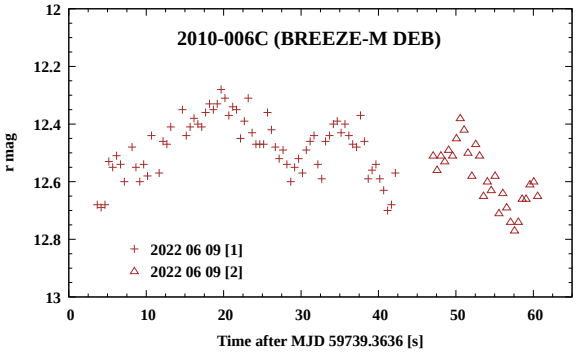

Figure 5. Light curve of the two streaks caused by 2010-006C.

5.4. 1991-033C (COSMOS 2145)

Another interesting object encountered during the preparation of the machine learning algorithm can be seen in Figure 6. The streak presents two distinctive lines parallel to each other. After correlation with the space-track catalogue, we have found the streak to correspond to the object 1991-033C (COSMOS 2145), part of the Strela-3 constellation.

The satellite is a former communication satellite launched in 1991 by the Soviet Union. Interestingly,

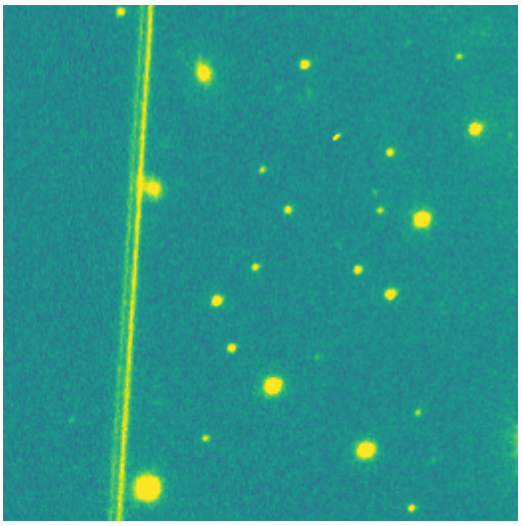

Figure 6. Streak of COSMOS 2145 taken on 2022/03/11.

Strela-3 satellites carry a gravity-gradient beam for stabilization and we believe that OmegaCAM was able to resolve the satellite, hence the characteristic two lines streak. To validate this assumption we performed a measure of the across dimension of the streak to obtain an estimate of the main body and beam length. Knowing the exact positions of the satellite and observer and assuming that the gravity gradient boom is pointing towards the center of earth, we estimate the total system to be $\sim$13 m long, for a beam length of the order of 10 m. These estimations correspond to the expected average dimensions of the satellite and give us great hope for the successful resolution of other space objects.

6. CONCLUSIONS AND FUTURE WORK

This work demonstrates the great value that data archives from large aperture telescopes have for the study of space debris. The high sensitivity of the OmegaCAM imager allows to sample light curves at a high rate with no deadtime which is impossible when using traditional observation techniques that track the target and acquire series of images to obtain light curves. Also, the high angular resolution is an advantage over conventional surveillance and tracking telescopes. OmegaCAM would resolve an object of 1 m at 600 km with 12 pixels. The example of the Strela-3 satellite, that was observed at a range of 1506 km, demonstrates how we can utilize the high resolution to estimate the size of a resolved target directly from the streaks.

These results encourage us to continue developing our detection methods, further automatize photometric reduction and implement more sophisticated methods to analyze the light curves. We will also implement initial orbit determination methods for streaks that can not be identified with known objects. This makes it possible to link these streaks to identify multiple observations of the same object and will allow us to determine rotation periods longer than the duration of a single observation and identify changes in the rotation period. Multiple observations of the same object can also be used to reconstruct the object's phase curve which can be used to estimate its size. The astronomical data archives typically contain observations in multiple pass bands. Analyzing the light curves from the same object in different bands may give further insight on the composition of its surface materials.

ACKNOWLEDGMENTS

The research reported in this article was supported by the Swiss National Science Foundation (SNSF) via the Bridge Discovery grant 194729. We would like to thank Stefano Mottola for providing us with his implementation of the FALC algorithm and Dr Olivier Hainaut for his advice.

REFERENCES

1. Kessler D. J., Cour-Palais B. G., (1978). *Collision frequency of artificial satellites: The creation of a debris belt*, Journal of Geophysical Research
2. Bonnal C., Ruault J.-M. and Desjean M.-C., (2013). *Active debris removal: Recent progress and current trends*, Acta Astronautica
3. Blake J. A., Chote P. et al., (2021). *DebrisWatch I: A survey of faint geosynchronous debris*, Advances in Space Research
4. Šilha J., (2020). *Space Debris: Optical Measurements*, Reviews in Frontiers of Modern Astrophysics: From Space Debris to Cosmology
5. Arnaboldi M. et al., (2016). *Public surveys at ESO*, Observatory Operations: Strategies, Processes, and Systems VI
6. Dey A. et al., (2019). *Overview of the DESI Legacy Imaging Surveys*, The Astronomical Journal
7. Frank J. M. et al., (2019). *The Zwicky Transient Facility: Data Processing, Products, and Archive*, The Astronomical Journal
8. Kuijken, K., (2011). *OmegaCAM: ESO's Newest Imager*, The Messenger
9. Diehl T., (2012). *The Dark Energy Survey Camera (DECam)*, Physics Procedia
10. Šilha J., Pittet J.-N., Hamara M., Schildknecht T., (2018). *Apparent rotation properties of space debris extracted from photometric measurements*, Advances in Space Research
11. Papushev P., Karavaev Yu., Mishina M., (2009). *Investigations of the evolution of optical characteristics and dynamics of proper rotation of uncontrolled geostationary artificial satellites*, Advances in Space Research

12. Williams J. G., McCue G. A., (1966). *An analysis of satellite optical characteristics data*, Planetary and Space Science
13. Krisciunas K., Schaefer B. E., (1991). *A model of the brightness of moonlight*, Publications of the Astronomical Society of the Pacific
14. Mark K. M., Mark M., (2008). *A New Bond Albedo for Performing Orbital Debris Brightness to Size Transformations*, Proceedings of the 59th International Astronautical Congress
15. Željko I. et al., (2019). *LSST: From Science Drivers to Reference Design and Anticipated Data Products*, The Astrophysical Journal
16. Vandame B., (2001). *Fast Hough Transform for Robust Detection of Satellite Tracks*, Mining the Sky, Springer-Verlag
17. Hickson P., (2018). *A fast algorithm for the detection of faint orbital debris tracks in optical images*, Advances in Space Research
18. Danarianto M. D., Maharani A. M., Falah B. M., Rohmah F., (2021). *Prototype of automatic satellite streak detection, identification and initial orbit determination pipeline from optical observation*, Journal of Physics
19. Duev D. A. et al., (2019). *DeepStreaks: identifying fast-moving objects in the Zwicky Transient Facility data with deep learning*, Monthly Notices of the Royal Astronomical Society
20. Ye Q. et al., (2019). *Toward Efficient Detection of Small Near-Earth Asteroids Using the ZwickyTransient Facility(ZTF)*, Publications of the Astronomical Society of the Pacific
21. Pöntinen M. et al., (2020). *Euclid: Identification of asteroid streaks in simulated images using StreakDet software*, Astronomy & Astrophysics
22. Lieu M., Conversi L., Altieri B., Carry, B., (2019). *Detecting Solar system objects with convolutional neural networks*, Monthly Notices of the Royal Astronomical Society
23. Lin Y., Pintea S. L. van Gemert J. C., (2020). *Deep Hough-Transform Line Priors*, arXiv
24. Iglovikov, V. and Shvets A., (2018). *TernausNet: U-Net with VGG11 Encoder Pre-Trained on ImageNet for Image Segmentation (Version 1)*, arXiv
25. Ronneberger O., Fischer P. and Brox T., (2015). *U-Net: Convolutional Networks for Biomedical Image Segmentation*, Lecture Notes in Computer Science
26. Tabur V., (2007). *Fast Algorithms for Matching CCD Images to a Stellar Catalogue*, Publ. Astron. Soc. Australia
27. Scheirich P. et a., (2015). *The binary near-Earth Asteroid (175706) 1996 FG3 — An observational constraint on its orbital evolution*, Icarus
28. Miralda-Escudé J., (2002). *Orbital Perturbations of Transiting Planets: A Possible Method to Measure Stellar Quadrupoles and to Detect Earth-Mass Planets*, The Astrophysical Journal
29. Eyer L., Mowlavi N., (2008). *Variable stars across the observational HR diagram*, Journal of Physics: Conference Series
30. Harris A. W. et a., (1989). *Photoelectric observations of asteroids 3, 24, 60, 261, and 863*, Icarus
31. Chote P., Blake J., Pollacco D., (2019). *Precision Optical Light Curves of LEO and GEO Objects* , Advanced Maui Optical and Space Surveillance Technologies Conference
32. Evans D. W. et a., (2018). *Gaia Data Release 2. The photometric content and validation*, Astronomy & Astrophysics
33. Pravec P. et a., (2000). *Two-Period Lightcurves of 1996 FG_3, 1998 PG, and (5407) 1992 AX: One Probable and Two Possible Binary Asteroids*, Icarus
34. Mueller B., (2002). *The Diagnosis of Complex Rotation in the Lightcurve of 4179 Toutatis and Potential Applications to Other Asteroids and Bare Cometary Nuclei*, Icarus